Journal of Catalysis 286 (2012) 248–259

Contents lists available at SciVerse ScienceDirect

Journal of Catalysis

journal homepage: www.elsevier.com/locate/jcat

# Vapor phase butanal self-condensation over unsupported and supported alkaline earth metal oxides

Wenqin Shen, Geoffrey A. Tompsett, Rong Xing, W. Curtis Conner Jr., George W. Huber *

*Department of Chemical Engineering, University of Massachusetts, Amherst, MA 01003, United States*

ARTICLE INFO

*Article history:*
Received 20 July 2011
Revised 8 November 2011
Accepted 11 November 2011
Available online 22 December 2011

*Keywords:*
Vapor phase butanal condensation
Supported alkaline earth metal oxides
Reaction network
Acid/base bifunctional catalysts
$CO_2$ and $NH_3$-TPD
TPD-DRIFTS

ABSTRACT

Vapor phase butanal condensation was studied over well-characterized MgO, $MgO/SiO_2$, $SrO/SiO_2$, $MgO—SrO/SiO_2$ and MgO/HY in a fixed-bed flow reactor. $CO_2$-TPD showed that the base strength and the number of basic sites decreased when the alkaline earth metal oxides were supported on silica. $NH_3$-TPD illustrated that new acid sites were generated when the alkaline metal oxides were supported on silica. The primary product for all catalysts was 2-ethyl-2-hexenal (EHEA) produced by aldol condensation of butanal. Side reactions produced several other products including butanoic acid, heptanone, 2-ethyl-2-hexenol, butanoic acid 2-ethyl-2-hexenol ester and 2,4,-diethyl-2-,4-octandienel by reactions including the Tishchenko cross esterification reactions, double aldol addition, ester hydrolysis, ketonization, cyclization and dehydration. As compared to the unsupported MgO, the silica supported MgO, SrO and MgO—SrO and MgO/HY exhibited an almost five times higher activity, a higher stability and an improved selectivity. This indicates that both acid and base sites are needed to achieve good catalytic performance for gas phase aldol condensation reactions. Catalyst activation and deactivation mechanisms were studied by butanal-TPD-DRIFTS and butanoic acid TPD-TGA. At temperatures below 300 °C, all catalysts deactivated due to poisoning by the butanoic acid, which was produced as a by-product. The weak bonding of the adsorbed species on the $MgO/SiO_2$ surface contributed to the improved stability of the catalyst for vapor phase butanal condensation.



## 1. Introduction

The sustainable biomass economy requires the development of different combinations of processes to lower the cost of producing fuels and chemicals from lignocellulosic biomass [1–3]. Carbon—carbon bond formation is one of the key reactions that are required to convert smaller biomass derived molecules into larger liquid fuels that could fit seamlessly into the diesel or jet fuel infrastructure [4,5]. One biomass conversion process developed by Dumesic and coworkers [5–7] involves sugar conversion into monofunctional compounds including alcohols, ketones, carboxylic acids and heterocyclic compounds in the range of C4–C6. These monofunctional small oxygenates are then converted into larger compounds by C—C bond formation reactions followed by hydrodeoxygenation to produce liquid fuels. The carbohydrate feedstock to this process is typically 5–6 carbons in length, and the process allows the production of jet and diesel fuels that are 8–18 carbons in length [5–7]. The C—C bond formation between small oxygenates can take place by both aldol condensation and ketonization. Aldol condensation occurs between aldehydes and/or ketones. For example, the ketone fraction of these monofunctional compounds can be coupled by C—C bond forming to produce larger ketones by aldol condensation over a Pd/Ce—Zr catalyst [8]. Furaldehydes can be coupled with acetone or propanal for the production of diesel range molecules over nitrogen substituted zeolites [9]. Ketonization occurs between carboxylic acids and esters to produce larger molecular ketones with the release of $CO_2$ and $H_2O$ over a $CeZrO_x$ catalyst [10,11].

Aldol condensations are industrially important reactions and can be catalyzed by acid, base and acid–base bifunctional catalysts [12,13]. A number of researchers have studied acetone self-condensation in both liquid and gas phases [14–22]. The reaction network for acetone self-condensation over acid–base bifunctional catalysts involves aldol addition, Michael addition, cracking, ketonization, dehydration, oligomerization, etc. as reported by Lippert et al. [22].

The aldol condensations of lower aldehydes have been studied over a number of solid catalysts including alkaline earth metal oxides [23], supported alkali catalysts [23–25], acidic zeolites [26], alkali modified zeolites [23,25,27–29], MgAl-hydrotalcites [25], anionic clay [21,25,30], $ZrO_2$ [31], sulfate modified $ZrO_2$ [31], lanthanum oxide [14], niobium oxide [18,32], cerium oxide [33], tita-

* Corresponding author.
*E-mail address:* huber@ecs.umass.edu (G.W. Huber).

0021-9517/$ - see front matter © 2011 Elsevier Inc. All rights reserved.
doi:10.1016/j.jcat.2011.11.009

nium oxide [16,17,34,35] and uranium oxide [36]. Hattori and coworkers [23,37] conducted liquid phase butanal condensation reactions at 0 °C and 50 °C over alkaline metal oxides (MgO, CaO and SrO), $ZrO_2$, $La_2O_3$, alumina supported alkaline catalysts and alkaline metal ion-exchanged zeolite X (M/MX, where M is Na, K, Rb). Alkali ion-exchanged and ion-added zeolites (Na/NaX, K/KX) showed the highest activity with about 60% conversion of butanal at 50 °C for 5 h reaction. $ZrO_2$ and $La_2O_3$ showed very low activity. The order of activity based on a unit surface area over alkaline metal oxides was SrO > CaO > MgO, which is in accordance with the base strength.

Several researchers have also studied aldol condensation of lower aldehydes in the vapor phase [26,28,29,31]. Ji et al. [31] studied the vapor phase acetaldehyde condensation over several types of solid catalysts. It was found that all the unsupported metal oxides had low activity or poor stability. Silica supported alkali metal oxides could catalyze aldol condensation of acetaldehyde with moderate conversion to produce crotonaldehyde as well as crotyl alcohol with selectivities of about 90%. Di Cosimo and Apesteguía [20] studied the deactivation of acetone over MgO and alkali-promoted MgO catalysts (Li/MgO, Na/MgO, K/MgO and Cs/MgO) during the vapor phase acetone condensation and proposed that the deactivation of the catalysts was caused by the formation of coke. The stronger base strength of the alkali promoter, the higher the deactivation rate of the catalyst. Several acidic zeolites including Y type zeolites, ZSM-5, mordenite, zeolite MFI and alkali modified zeolites have also been investigated for vapor phase aldol condensations of lower aldehydes [26–29]. Rode et al. [29] found that Cs/NaY was the most active catalyst among Cs/NaY, NaY, Li/NaY, MgO and $Al_2O_3$, showing a 100% selectivity to 2-ethyl-2-hexenal (EHEA) in the vapor phase butanal condensation, which could be attributed to the acid–base bifunctionality as they proposed. The authors verified this hypothesis by selective poisoning of either acidic or basic sites. King et al. [24,38] showed that the catalytic conversion of butanal could be increased up to 82% (compared to 58% maximum) by adding Pd to a $Na/SiO_2$ catalyst during the first 4 h of gas phase condensation. However, the Pd catalyst deactivated quickly for some unknown reason. More recently, Kunkes et al. [8] conducted gas phase 2-hexanone self-condensation/hydrogenation reactions over a $Pd/CeZrO_x$ catalyst at 300–400 °C and found that the addition of primary alcohols and carboxylic acid as well as water and $CO_2$ reversibly inhibited the self-coupling activity of 2-hexanone.

From the above literature review, it can be concluded that most vapor phase aldol condensation catalysts with primarily either very strong acid or very strong base sites only, deactivated quickly.

Gas phase aldehyde condensation has been studied thoroughly in the past decades over several different types of catalysts (solid base, acid, acid–base bifunctional catalysts and redox catalysts); however, there is no detailed understanding of the deactivation mechanisms. Furthermore, the reaction pathways are still debated with some studies, showing a very simple product distribution [14,23,28,29,31,32,38], while several other researchers report a number of complicated side reactions [8,27,33–35]. It is generally agreed that these condensation reactions are enhanced by acid–base bifunctional catalysts with catalysts that contain both acid and base sites [39–42]. However, this hypothesis was mainly based on the observation of reaction kinetics without further spectroscopic support. It is not clear why the unsupported catalysts show relatively low activity and stability. It is also not clear how the catalysts undergo deactivation. The objective of this paper is to study butanal vapor phase condensation with a series of well-characterized MgO and SrO based catalysts with the goals of identifying the reaction network, showing the catalyst deactivation and activation mechanism and providing insight for improved catalysts for this reaction.

## 2. Experimental

### 2.1. Materials

Butanal (99%, Acros Organics) was used for vapor phase reaction without further purification. Butanoic acid (99%+, Acros Organics), 4-heptanone (98%, Acros Organics), butyl butyrate (98%, Acros Organics), 2-ethyl-2-hexenal (Acros Organics), butanol (99.5% Acros Organics), heptene (98%, Acros Organics, heptanes (99.5%, Acros Organics) and *n*-octane (97%, Acros Organics) were used for GC calibration. Fumed silica (CAB-O-SIL, untreated) and HY (CBV720, Zeolyst International) were used as catalyst support materials.

### 2.2. Catalyst preparation

MgO was prepared by precipitation of $Mg(NO_3)_2{\cdot}6H_2O$ (Aldrich) from an aqueous solution with NaOH. Typically, 51.3 g of magnesium nitrate hexahydrate was dissolved in 1 L of deionized water. A 25 wt.% NaOH aqueous solution in a separation funnel was added dropwise into the mixed solution with vigorous stirring until the pH was equal to 10. The resulting gel was aged at room temperature for 72 h and separated by vacuum filtration. The precipitate was thoroughly washed with deionized water at least four times, dried in an oven at 120 °C overnight and calcined in 100 mL/min air flow at 550 °C for 3 h after a 3 h heating ramp. The supported catalysts were prepared by the impregnation method. Typically, the desired amounts of catalyst precursors ($Mg(NO_3)_2{\cdot}6H_2O$ Aldrich, $Sr(NO_3)_2$ Fisher Scientific) were first dissolved in 50 mL deionized water, and the catalyst support (5 g) was then added into the solution with vigorous stirring for 2 h. The resulting mixture was dried slowly by using a rotary evaporator (BUCHI Inc.) operated at 23 mbar vacuum with a bath temperature of 40 °C for 4–6 h. The dried materials were next calcined in a furnace at 550 °C for 4 h with a 10 °C/min heating ramp rate in a 100 mL/min air flow, and the fresh calcined samples were finally transferred into a sealed container flushed with He and stored in a desiccator cabinet.

### 2.3. Butanal condensation reaction

Butanal condensation reactions were conducted in a fixed-bed plug-flow reactor. Typically, 200 mg of catalyst was loaded at the center of a quartz tube reactor with ½ inch outside diameter and supported by a quartz frit. Butanal was fed into the reactor using a syringe pump (Fisher Scientific) with a typical flow rate of 1.2 mL/h. The liquid feed was distributed by an 8 cm length quartz bead bed above the catalyst bed, evaporated and carried into the catalyst bed by a 60 mL/min He flow. The catalyst bed temperature and furnace temperature were controlled and monitored by two temperature controllers (EZ-ZONE PM, Watlow), respectively. The inlet gas flow was controlled by a mass flow controller (5850E, Brooks Instrument). Before reaction, the catalyst was first degassed at 350 °C for 2 h with a 10 °C/min heating rate in a 60 mL/min He flow. The reactions were typically conducted at 300 °C for 2 h in a 60 mL/min He flow. The un-reacted butanal and products were captured by liquid nitrogen and diluted with methanol before analysis. The products were identified and analyzed by gas chromatography/mass spectrometry (GC/MS; Shimadzu GC/MS-2100 with a DB-5 column from Alltech). The catalysts were evaluated based on their catalytic performances. The definition of butanal conversion and product selectivity is as follows:

$$\text{Conversion}\% = \frac{\text{moles of butanal consumed}}{\text{moles of butanal input}} \times 100\%$$

$$\text{Selectivity}\% = \frac{M \times \text{moles of product}}{\text{moles of butanal consumed}} \times 100\%$$

$$\text{Yield}\% = \frac{M \times \text{moles of product}}{\text{moles of butanal input}} \times 100\% = \text{Conversion}\% = \frac{\text{Selectivity}\%}{100}$$

where $M$ represents the reaction stoichiometry.

### 2.4. Characterization

X-ray diffraction (XRD) patterns were measured with a Philips X'Pert professional diffractometer using a nickel filtered Cu Kα source at a wavelength of 1.54 Å. An accelerating voltage of 45 kV and a current of 40 mA were used. A slit width of 0.5° was used on the source. Scans were collected using an X'Celerator detector.

Nitrogen adsorption experiments were conducted by using the Autosorb-1 MC instrument from Quantachrome Instruments. The BET surface areas of the catalysts were calculated by multipoint BET method (seven points) in the relative pressure range from 0.01 to 0.3, or using the Dubinin–Radushkevich method.

Temperature programmed desorption (TPD) of $CO_2$ and $NH_3$ was used to characterize the basic and acid sites over the studied catalysts, respectively. The TPD experiments were conducted by using a ChemBET Pulsar TPR/TPD instrument (Quantachrome Instruments) with a built-in TCD detector. Typically, 300 mg catalyst was used in each measurement. The catalyst was first purged with He (UHP grade, Airgas) at 550 °C for 1 h with a 10 °C/min heating ramp rate, then cooled down to room temperature. A flow of $CO_2$ (research grade, Airgas) or $NH_3$ (electronic grade, Airgas) was introduced into the tubular catalyst bed for 10–30 min at room temperature for $CO_2$ adsorption and 100 °C for ammonia adsorption, respectively. After purging the catalyst bed for about 30 min with He to evacuate the physisorbed $CO_2$ or $NH_3$, the catalyst was heated up to 550 °C with a 10 °C/min heating ramp rate. The change in thermal conductivity due to the concentration change of $CO_2$ or $NH_3$ in the effluent was recorded. The TPD profile was deconvoluted by using Gaussian multipeak fitting function built-in OriginPro7.5 software. The fitting parameter R squared was larger than 0.999 for each fitting.

The butanoic acid TPD-TGA experiment over the $MgO/SiO_2$ and $SrO/SiO_2$ catalysts was conducted by using a thermo-gravimetric analyzer (TA Instruments, SDTQ600). Typically, the catalyst was first purged in a fixed-bed flow reactor in a 60 mL/min ultra-high purity He flow at 550 °C for 2 h and then cooled to 50 °C. The butanoic acid at room temperature was carried into the catalyst bed by a 60 mL/min ultra-high purity He flow. The catalyst was purged for 6 h and then evacuated for 1 h at room temperature in a He flow to release the physically adsorbed butanoic acid. Next, the catalyst was quickly transferred into the TGA sample container and was further degassed at 50 °C for 1 h in the TGA system. The butanoic acid saturated catalyst was heated up to 450 °C with a heating rate of 10 °C/min in a 100 mL/min He flow.

A Bruker Equinox-55 Fourier transform infrared spectrometer equipped with diffuse reflectance (DRIFTS) accessory (Praying Mantis™ diffuse reflectance accessory, Harrick Scientific) was used for the TPD-FTIR experiments. The reaction chamber (HVC-DRP, Harrick Scientific) with KBr windows allows gas flow and heating of the catalyst sample while simultaneous measurement of infrared spectra. The chamber can be heated up to 600 °C, and the temperature was controlled by a Watlow (EZ-ZONE MP) temperature controller. A DTGS detector was used. The spectra were recorded between 4000 $cm^{-1}$ and 400 $cm^{-1}$ and collected by averaging 50 scans at a resolution of 4 $cm^{-1}$. KBr powder was used as the spectral background. About 50 mg of catalyst was loaded into the reaction chamber for each test. The catalyst was first calcined at 500 °C in a 20 mL/min air flow and cooled down to 50 °C in a 20 mL/min He flow. Butanal was absorbed at 50 °C for 1 h and purged under He for 30 min. The TPD was studied from 50 °C to 500 °C with 10 °C intervals.

## 3. Results and discussion

### 3.1. Characterization

A range of characterization techniques were used to analyze the catalysts including XRD, $N_2$ adsorption, $NH_3$-TPD and $CO_2$-TPD. XRD data (see Supporting Fig. S1) show that all the silica supported catalysts are amorphous. This indicates that MgO and SrO were either well dispersed on the silica support or formed an amorphous magnesium or strontium silicate phase. The XRD pattern of MgO/HY shows only the reflections for the crystalline HY support material.

Table 1 summarizes the calculated BET surface areas, $CO_2$ and $NH_3$-TPD measurements of the catalyst materials. The BET surface areas of the silica supported catalysts were similar, at about 110–130 $m^2/g$. The BET surface area of the calcined and spent $MgO/SiO_2$ catalyst decreased slightly from 123 $m^2/g$ to 91 $m^2/g$. The decrease in the BET surface area is probably due to coke formation on the spent catalyst. The BET surface area of MgO/HY is not valid because HY is microporous ($C_{BET} = -38$). The surface area of MgO/HY was instead calculated using the Dubinin–Radushkevich equation to give 551 $m^2/g$. As we can see, the surface area of MgO/HY is significantly higher than the silica supported catalyst due to the microporosity of the zeolite material.

The overall $CO_2$ and $NH_3$ uptakes based on the total catalyst weight are also listed in Table 1. The $CO_2$ uptake of the MgO catalyst was 181 μmol/g cat. All the supported catalysts had much lower $CO_2$ uptake than the unsupported MgO catalyst, mostly due to the dilution effect of the support. There was no $CO_2$ desorption observed over the $SiO_2$ support alone. Among all catalysts, MgO/HY had the highest $NH_3$ uptake of 610 μmol/g cat., followed by MgO—$SrO/SiO_2$ and $MgO/SiO_2$. MgO showed no $NH_3$ uptake.

Fig. 1 shows the $CO_2$ and $NH_3$-TPD profiles for the catalysts studied. Table 2 lists the total $CO_2$ and $NH_3$ uptakes on the basis of metal oxide (MO) and the corresponding concentrations for the different types of acid/base sites. Compared to the supported catalysts, unsupported MgO had a much broader $CO_2$ desorption range from a temperature of 112 °C to 338 °C in the $CO_2$-TPD profile. The low-temperature $CO_2$ desorption (about 100 °C) was related to the bicarbonate species, the medium temperature desorption (about 200 °C) was related to bidentate carbonate and high-temperature desorption (above 300 °C) was related to the unidentate species, respectively [43–45]. The silica supported alkaline earth metal oxide catalysts showed a much smaller desorption at temperature of 200–340 °C. Three $CO_2$ desorption peaks were observed for the supported catalysts at 100–110 °C, 140–150 °C and 190–200 °C, indicating three types of sites interacting with $CO_2$. These peaks are probably bicarbonate (two types) and bidentate carbonate type species. The absence of unidentate carbonate (low-coordinated $O^{2-}$) on the strongest basic site might be caused by the dispersion of magnesium or strontium on the silica support. The overall $CO_2$ uptake on an alkaline earth metal oxide basis was three times higher for the $SrO/SiO_2$ (18.3 μmol/mmol SrO) compared to the $MgO/SiO_2$ catalyst (5.9 μmol/mmol MO). The MgO—$SrO/SiO_2$ (26.2 μmol/mmol MO) had the highest $CO_2$ uptake. The ratio of the high-temperature desorption peak, at above ~200 °C, increased from 0.17 for $MgO/SiO_2$ to 0.21 for $SrO/SiO_2$ and to

**Table 1**
$N_2$, $CO_2$ and $NH_3$ adsorption/desorption measurements for catalysts used in this study. (All catalysts were calcined at 550 °C).

| Catalyst | Metal oxide loading[a] (wt.%) | BET surface area ($m^2$/g) | | Basic sites[b] (μmol $CO_2$/g cat.) | Acid sites[c] (μmol $NH_3$/g cat.) |
|---|---|---|---|---|---|
| | | Fresh | Spent[c] | | |
| MgO | 100 | 95 | – | 181 | 0 |
| $MgO/SiO_2$ | 20 | 123 | 91 | 24 | 156 |
| $SrO/SiO_2$ | 20 | 130 | – | 24 | 87 |
| $MgO—SrO/SiO_2$ | 40 | 108 | – | 104 | 204 |
| MgO/HY | 40 | 551[d] | – | 87 | 610 |
| $SiO_2$ | 100 | 150 | – | 0 | 7 |

[a] Metal oxide loading refers to the weight of metal oxide over the weight of support.
[b] The basic sites were measured based on the $CO_2$-TPD.
[c] The acid sites were measured based on the $NH_3$-TPD.
[d] Calculated using DR method.

**Table 2**
List of the total $CO_2$ and $NH_3$ uptakes on a metal oxide (MO) basis and the corresponding concentrations for the different types of acid/base sites.

| Catalyst | MgO | $MgO/SiO_2$ | $SrO/SiO_2$ | $MgO—SrO/SiO_2$ | MgO/HY | $SiO_2$ |
|---|---|---|---|---|---|---|
| Total (μmol $CO_2$/mmol MO) | 7.2 | 5.9 | 18.3 | 26.2 | 12.2 | – |
| $T_1$ (100–110 °C) | 0.125 | 0.44 | 0.34 | 0.19 | 0.26 | – |
| $T_2$ (140–150 °C) | 0.29 | 0.39 | 0.43 | 0.38 | 0.49 | – |
| $T_3$ (190–210 °C) | 0.07 | 0.17 | – | 0.42 | 0.14 | – |
| $T_4$ (~230 °C) | 0.40 | – | 0.21 | – | 0.12 | – |
| $T_5$ (~340 °C) | 0.11 | – | – | – | – | – |
| Total (μmol $NH_3$/mmol MO) | – | 37.6 | 54.2 | 35.2 | 73.3 | 0.4 |
| $T_1$ (180–210 °C) | – | – | 0.30 | 0.22 | 0.20 | 1 |
| $T_2$ (240–260 °C) | – | 0.21 | 0.42 | 0.24 | 0.22 | – |
| $T_3$ (~280–300 °C) | – | 0.33 | – | 0.29 | 0.28 | – |
| $T_4$ (>340 °C) | – | 0.46 | 0.28 | 0.25 | 0.30 | – |

0.42 for $SrO—MgO/SiO_2$. This indicates that the mixture of SrO and MgO is a stronger base catalyst compared to the silica supported pure MgO and SrO catalysts.

Ammonia is a good electron donor and proton acceptor; thus, it is a probe of Lewis and Brønsted acid sites over solid catalyst surfaces [46]. Tsuji and coworker [23] reported $NH_3$ desorption over MgO at ~100 °C due to the Lewis acid site of $Mg^{2+}$ from $Mg^{2+}—O^{2-}$ pair. The $NH_3$ desorption was conducted at room temperature in that study. There is no $NH_3$ desorption over MgO at our experimental operating conditions ($NH_3$ adsorption and evacuation was performed at 100 °C). A very small amount of $NH_3$ uptake (6.7 μmol/g cat.) was observed over $SiO_2$ support at ~210 °C, probably due to the weak Lewis acid sites from surface silanol groups. The silica supported MgO and SrO catalysts had a dramatically increased $NH_3$ uptake of 156 and 87 μmol/g catalyst, respectively, indicating that extra acid sites were formed when MgO and SrO were supported on $SiO_2$. This generation of strong acid sites over silica-magnesia mixed oxides was also observed by López and coworkers [47]. The $NH_3$-TPD profiles show similar asymmetric shapes with broadened peaks for all the silica supported catalysts. The total $NH_3$ uptake over $MgO—SrO/SiO_2$ was about 203 μmol/g cat., slightly less than the $NH_3$ uptakes for $MgO/SiO_2$ plus $SrO/SiO_2$. This probably

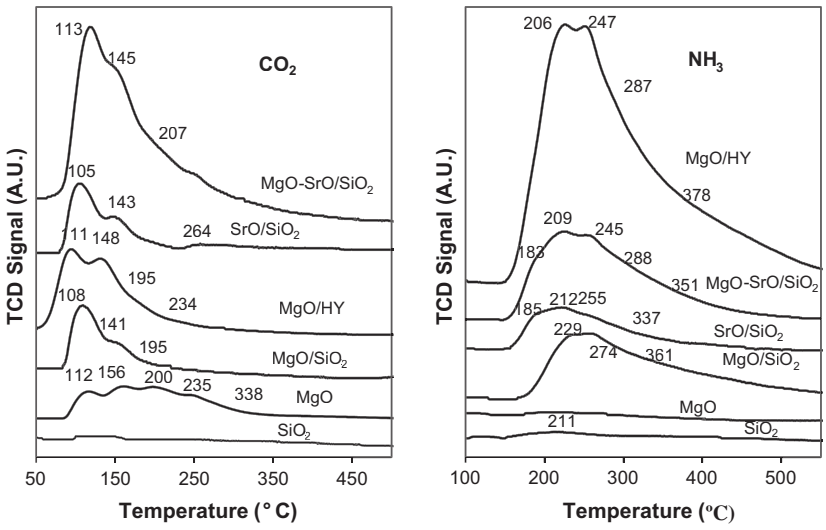


**Fig. 1.** $CO_2$-TPD and $NH_3$-TPD thermograms of the studied catalysts with the desorption temperatures on each profile. All the signals were related to 300 mg of the studied catalyst, and the signal for $CO_2$-TPD of MgO was divided by 6 (50 mg).

indicates that the number of acid sites is also related to the loading of metal oxide over the silica supported alkaline metal oxide catalysts. The $NH_3$ uptake over MgO/HY was much higher than that of silica supported MgO due to the extra acid sites introduced by the acidic HY support. $MgO/SiO_2$ had the highest concentration of the strong acid sites that desorbed at temperatures above 340 °C. The acid strength over MgO—$SrO/SiO_2$ was similar to a mixed character of both $MgO/SiO_2$ and $SrO/SiO_2$.

A number of changes have been observed as the metal oxide is added to the silica support. The base strength and the basic site density (defined by the number of basic sites over catalyst surface area) decrease dramatically. Strong acid sites are apparently generated when the metal oxide is mixed with silica. The modification of silica with acid and base oxides and the characterization of the acid–base character have been extensively studied in the literature for many years [47–53], consistent with our experimental results.

### 3.2. Butanal condensation reaction

Fig. 2 shows the time-on-stream butanal conversion over the MgO, $MgO/SiO_2$, $SrO/SiO_2$, MgO—$SrO/SiO_2$ and MgO/HY catalysts. The reaction was conducted at 300 °C for 2 h. A summary of butanal conversions and product yields is shown in Table 3. The MgO catalyst showed very low activity for butanal self-condensation with less than 4% conversion at 15 min reaction. This catalyst also deactivated to less than 1% conversion after 2 h reaction. The yield of EHEA over the MgO catalyst was initially 3.1%, and the side products were heptanone and 2-ethyl-2-hexenol (EHEO) with about 0.3% and 0.2% yields, respectively. However, the yield of EHEA decreased to 0.2% after 2 h reaction. The only side product observed after 2 h reaction over MgO was butanoic acid with 0.1% yield. The silica supported MgO catalyst showed dramatically improved performance with 17.4% butanal conversion at 15 min reaction. The yield of EHEA was 14.8% compared to 3.1% over MgO, and the yields of the side products EHEO, heptanone (HPO) and 2-ethyl-hexanal (EHAA) were 1.4%, 0.1% and 0.1%, respectively. The $MgO/SiO_2$ catalyst deactivated to 5.1% conversion of butanal after 2 h reaction with a butanoic acid yield of about 0.1%. $SrO/SiO_2$ showed similar activity compared to $MgO/SiO_2$ with about 17.6% conversion of butanal, but a slightly increased yield (0.7%) of double aldol addition product 2,4-diethyl-2,4-octadienal (EOEA) and slightly decreased yield of EHEO. Compared to $MgO/SiO_2$, SrO—$MgO/SiO_2$ showed further increased activity with a 36.6% conversion of butanal, and about 28.8% yield of EHEA, 2.4% yield of EHEO, and significant amount of product EOEA (about 5.1% yield), at 15 min reaction MgO/HY exhibited higher activity for butanal conversion than $MgO/SiO_2$ with about 34% conversion initially. However, the yield of EHEA was only 18.3% for the MgO/HY catalyst. All the catalysts studied including the unsupported and supported alkaline metal oxide catalysts deactivated with time-on-stream. There were noticeable amounts of butanoic acid observed in the effluent, especially for the deactivated catalysts. There was no heptanone observed over the catalysts that contained SrO.

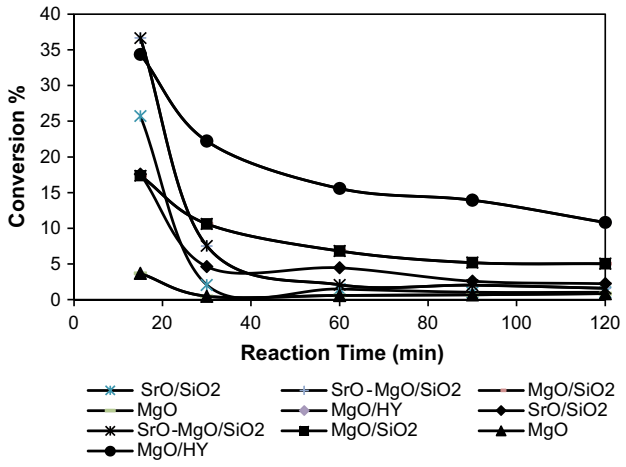


**Fig. 2.** Time-on-stream butanal conversion over the studied catalysts at 300 °C and 1 atm. The catalyst loading was 200 mg, and the butanal feeding rate was 1.2 mL/h with a 60 mL/min He co-feed.

There is no simple relationship between the catalytic activity for vapor phase butanal condensation and acid/base sites concentrations for these supported alkaline earth metal oxide catalysts. Numerous previous reports showed that the reaction could be catalyzed by acid–base bifunctional catalysts, which is consistent with this study [23,29,39,41,54].

### 3.3. Reaction network

According to prior studies, there are two key reactions for butanal condensation in the gas phase including aldol condensation and Tishchenko self- and cross-esterification reactions. Tishchenko-type esterification reactions could be catalyzed on acid, base and acid–base bifunctional catalysts [23], the same with aldol condensation. Therefore, esterification reactions always compete with aldol condensation on the catalyst surface. As proposed by Tsuji et al. [23], the cross-esterification reaction was preferred to the self-esterification reaction due to a stearic or electronic effect resulting from the structure of the aldol condensation dimer product EHEA. Our experimental observations in this study are consistent with this previous report since there was no butanol produced (from hydrolysis of butyl butyrate) in the current experimental conditions, while significant amounts of 2-ethyl-2-hexenol and its isomer 2-ethyl-hexanal (from hydrolysis of cross-esterification product) were detected.[23].

Ji and coworkers [31] proposed that the alcohol was produced by the reduction of the aldehyde with surface hydrogen produced through a parallel reaction. Idriss et al. [34] proposed that a small fraction of the absorbed acetaldehyde could be completely decomposed to surface carbon, hydrogen and oxygen, thus providing the reduction and oxidation source. Since the reaction in this work was conducted in an inert atmosphere, the surface hydrogen source might be generated by the dissociation of water from dehydration of the aldol addition product. Moreover, ester hydrolysis could be easily catalyzed by either acid sites or basic sites. The observation of a small amount of butanoic acid over the deactivated catalyst in this study further confirmed the hypothesis of the hydrolysis mechanism of ester from Tishchenko reaction for the production of alcohols, specifically, 2-ethyl-2-hexenol here. Another debate is related to the C7 products. According to Idriss et al.'s proposed reaction network [33,34,55], the C7 alkenes were produced by reductive coupling of butanal. However, Luo and coworkers [35] pointed out that the reductive coupling preferred to occur on the reductive surface. The unsaturated aliphatic hydrocarbons were possibly generated from the secondary reactions of the aldol condensation product, such as dehydroxylation or decarboxylation. In other experiments, we performed furfural (which has no α-H and therefore self-aldol condensation reaction could not occur) condensation experiments in a He and $H_2$ atmosphere over $MgO/SiO_2$. The catalyst showed no activity at all for the reductive coupling reaction. Therefore, the C7 alkenes are most likely produced from hydrogenation/dehydration of heptanone from ketonization of butanoic acid. The observation of heptanone for gas phase butanal condensation was also confirmed by Rode et al. [29] from an FTIR study, consistent with our experimental observation.

**Table 3**
Butanal conversion and product yield over the studied catalysts. Reactions were conducted at 300 °C with butanal feeding rate of 1.2 mL/h and the catalyst loading of about 200 mg.

| Catalyst | Reaction $T$ (°C) | Reaction time (min) | Butanal conversion (%) | Product yield (%) | | | | | | | | |
|---|---|---|---|---|---|---|---|---|---|---|---|---|
| | | | | EHEA | C7AL | C8AL | BA | HPO | EHEO | EHAA | TEB | EOEA |
| MgO | 300 | 15 | 3.7 | 3.1 | – | – | – | 0.3 | 0.2 | – | – | – |
| | | 120 | 0.8 | 0.2 | – | – | 0.1 | – | – | – | – | – |
| $MgO/SiO_2$ | 300 | 15 | 17.4 | 14.8 | – | – | – | 0.1 | 1.4 | 0.1 | – | – |
| | | 120 | 5.1 | 4.3 | – | – | 0.1 | 0.1 | 0.1 | 0.4 | 0.1 | – |
| MgO/HY | 300 | 15 | 34.4 | 18.3 | – | 6.1 | – | 0.3 | 1.7 | 1.9 | 0.5 | 1.7 |
| | | 120 | 10.8 | 7.2 | – | 0.2 | 0.1 | 0.1 | 0.6 | 0.4 | – | 0.2 |
| $SrO/SiO_2$ | 300 | 15 | 17.6 | 15.3 | – | – | – | – | 0.9 | 0.1 | – | 0.7 |
| | | 120 | 2.3 | 2.0 | – | – | 0.1 | – | 0.1 | – | – | – |
| SrO—MgO/$SiO_2$ | 300 | 15 | 36.6 | 28.8 | – | – | – | – | 2.4 | 0.5 | – | 5.1 |
| | | 120 | 1.6 | 1.0 | – | – | 0.4 | – | 0.1 | 0.03 | – | – |

*Note*: EHEA: 2-ethyl-2-hexenal; C7AL: C7 alkanes; C8AL: C8 alkanes; BA: butanoic acid; HPO: heptanone; EHEO: 2-ethyl-2-hexenol; EHAA: 2-ethyl-hexanal; TEB: triethyl benzene; EOEA: 2,4-diethyl-2,4-octadienal.

Therefore, from the time-on-steam product yields over the studied catalysts and the discussions above, we proposed the reaction network for vapor phase butanal condensation as shown in Scheme 1, including aldol condensation, dehydration, Tishchenko self- and cross-esterification reactions, hydrolysis, isomerization, hydrogenation and ketonization. The primary reaction pathway is butanal self-condensation to generate β-hydroxyl aldehyde (BHA) followed by the dehydration reaction for the formation of α,β-unsaturated aldehyde EHEA. The EHEA can undergo dehydration/hydrogenation to form C8 alkanes or unsaturated C8 alkenes (C8AL), or EHEA can react with another butanal by a second aldol addition producing 2,4-diethyl-2,4-octadienal (EOEA). This product can undergo dehydration/cyclization to form 1,3,5-triethyl benzene (TBE). EHEA can also react with butanal by Tishchenko cross-esterification reaction for the generation of reaction intermediate butanoic acid 2-ethyl-2-hexenol ester (BAEHO), followed by hydrolysis to produce butanoic acid (BA) and 2-ethyl-2-hexenol (EHEO). Butanoic acid can further react to form heptanone (HPO) by ketonization. EHEO can be converted to 2-ethyl-hexanal (EHAA) by isomerization. The butyl butyrate (BBA) can be produced by Tishchenko self-esterification reaction of butanal. BBA can further undergo hydrolysis to butanoic acid and butanol or generate heptanone by ester ketonization. Heptanone undergoes hydrogenation/dehydration to form C7 alkenes (C7AL). Since there is no C8 acid produced in the effluent, the reaction intermediate (BAEHO) is the preferred product for the Tishchenko cross-esterification between EHEA and butanal. Another possible Tishchenko product from EHEA and butanal is 2-ethyl-2-hexenoic acid butyl ester, which was not shown in Scheme 1.

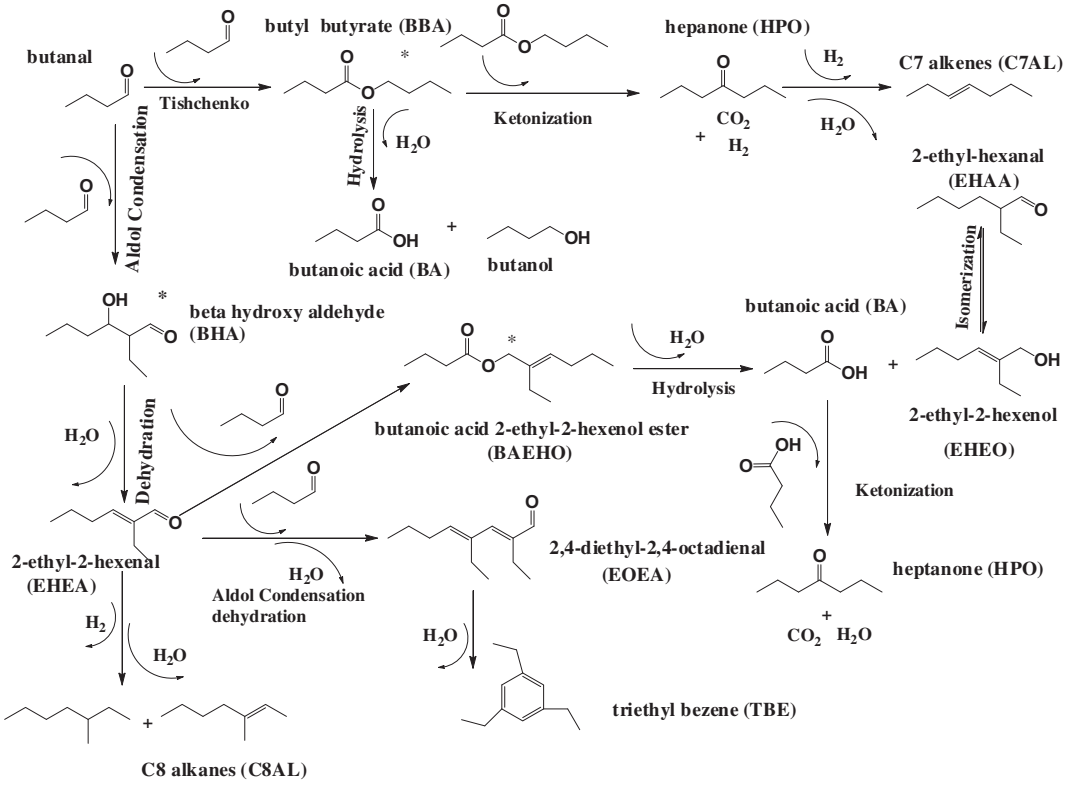


**Scheme 1.** Proposed reaction network for gas phase butanal condensation. The compounds with * represent reaction intermediates not observed in this study. The aldol condensation, Tishchenko esterification, ketonization and hydrolysis are able to be catalyzed by acid, base and acid/base bifunctional catalyst.

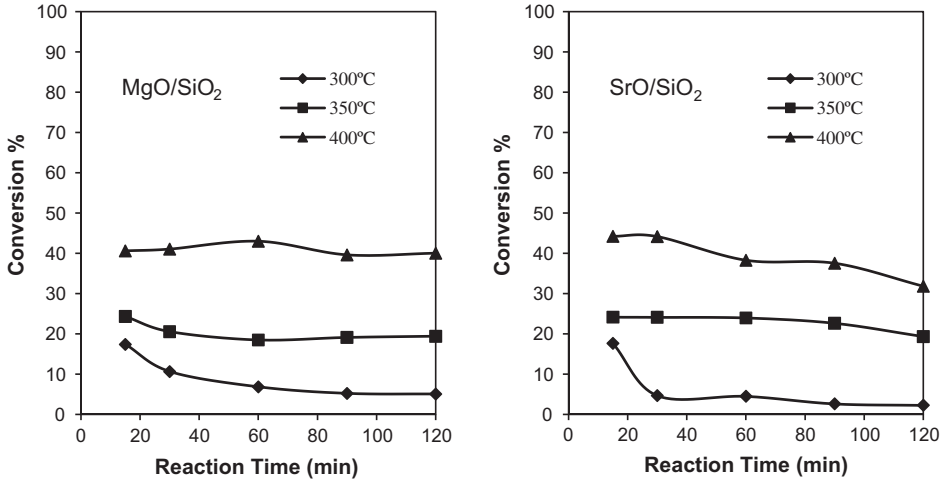


**Fig. 3.** Time-on-stream butanal conversion over $MgO/SiO_2$ and $SrO/SiO_2$ catalysts at the different operating temperatures. The catalyst loading was 200 mg, and the butanal feeding rate was 1.2 mL/min. Reactions were conducted in a helium atomsphere.

**Table 4**
Butanal conversion, catalyst apparent deactivation rate and product yields over $MgO/SiO_2$ and $SrO/SiO_2$ at different reaction temperatures.

| Catalyst | Reaction $T$ (°C) | Reaction time (min) | Butanal conversion (%) | Apparent deactivation rate ($min^{-1}$) | Product yield (%) | | | | | | | | |
|---|---|---|---|---|---|---|---|---|---|---|---|---|---|
| | | | | | EHEA | C7AL | C8AL | BA | HPO | EHEO | EHAA | TEB | EOEA |
| MgO/$SiO_2$ | 300 | 15 | 17.4 | 0.0067 | 14.8 | – | – | – | 0.05 | 1.40 | 0.07 | – | – |
| | 300 | 120 | 5.1 | | 4.3 | – | – | 0.10 | 0.04 | 0.35 | 0.07 | – | – |
| | 350 | 15 | 24.3 | 0.0019 | 18.2 | 0.44 | – | – | 0.29 | 2.28 | 0.12 | – | 2.40 |
| | 350 | 120 | 19.4 | | 14.0 | 0.35 | – | – | 0.29 | 1.78 | – | – | 0.74 |
| | 400 | 15 | 40.6 | 0.00014 | 18.8 | 0.89 | 2.96 | – | 0.97 | 3.37 | 0.93 | 0.12 | 4.06 |
| | 400 | 120 | 40.0 | | 23.0 | 0.64 | 1.68 | – | 1.32 | 4.08 | 0.84 | 0.18 | 3.56 |
| SrO/$SiO_2$ | 300 | 15 | 17.6 | 0.0072 | 15.3 | – | – | – | – | 0.93 | – | – | 0.72 |
| | 300 | 120 | 2.3 | | 2.0 | – | – | 0.10 | – | 0.14 | – | – | – |
| | 350 | 15 | 24.1 | 0.0017 | 19.0 | 0.80 | – | – | – | 1.86 | 0.02 | – | 1.08 |
| | 350 | 120 | 19.3 | | 15.7 | 0.29 | – | – | 0.06 | 1.62 | – | – | 0.27 |
| | 400 | 15 | 44.2 | 0.0023 | 28.8 | 0.22 | 0.66 | – | 0.30 | 4.15 | 0.71 | – | 3.45 |
| | 400 | 120 | 31.8 | | 23.8 | 0.45 | 0.13 | – | 0.29 | 3.31 | 0.16 | – | 1.21 |

*Note*: Apparent deactivation rate was defined by the conversion of butanal at 15 min minus the conversion at 120 min over the conversion at 15 min and reaction time (min). EHEA: 2-ethyl-2-hexenal; C7AL: C7 alkanes; C8AL: C8 alkanes; BA: butanoic acid; HPO: heptanone; EHEO: 2-ethyl-2-hexenol; EHAA: 2-ethyl-hexanal; TEB: triethyl benzene; EOEA: 2,4-diethyl-2,4-octadienal.

### 3.4. Effect of reaction temperature

The temperature effect on the catalytic performance of butanal condensation was studied over silica supported MgO and SrO catalysts at 300 °C, 350 °C and 400 °C as shown in Fig. 3 and Table 4. At 300 °C, $MgO/SiO_2$ showed the lowest activity and the highest apparent deactivation rate. The butanal conversion increased from 17% at 300 °C to 24% at 350 °C to 40% at 400 °C for $MgO/SiO_2$. This catalyst was stable at 400 °C. The yield of EHEA increased slightly from 15% at 300 °C to about 19% at 400 °C after 15 min reaction. The yields of other C8 products (C8AL, EHEO and EHAA) increased with increasing temperature as well. The yield of C12 products (EOEA and TEB) increased dramatically from 0% to 4.2% at 15 min reaction. Meanwhile, the yield of heptanone increased from 0.05% at 300 °C to 0.3% at 350 °C to approximate 1% at 400 °C, the C7 alkenes became noticeable with about 2% selectivity and butanoic acid production disappeared at the temperature above 350 °C. These results indicate that the ketonization reaction, the Tishchenko esterification reaction and the second aldol addition reaction were all promoted by the increased reaction temperature over $MgO/SiO_2$. $MgO/SiO_2$ was stable during 2 h operation at 400 °C, which was presumably due to the increased ketonization reaction that converted butanoic acid (strong adsorption species on basic sites) to heptanone. The effect of butanoic acid was further studied in the followed Sections 3.5 and 3.6. $SrO/SiO_2$ showed very similar behavior at different reaction temperatures as $MgO/SiO_2$. However, $SrO/SiO_2$ was less stable at the elevated temperature, and the C7 product selectivity (C7 AL and heptanone) was much less than $MgO/SiO_2$, indicating this catalyst had a lower reactivity toward ketonization. However, $SrO/SiO_2$ had high yield for the primary product EHEA with about 29% at 400 °C after 15 min reaction. The spent catalysts were black indicating that coke formation occurred with both catalysts, especially at 400 °C. Coking caused the slow deactivation of the catalysts at high operating temperatures, which was confirmed by in situ FTIR data as discussed in Section 3.7.

### 3.5. Effect of butanoic acid

The effect of butanoic acid on the catalytic performance of vapor phase butanal condensation was studied over $MgO/SiO_2$ at 300 °C and 400 °C as shown in Fig. 4 and Table 5. At 300 °C, the $MgO/SiO_2$ catalyst deactivated very rapidly with a co-feed of 1 vol.% butanoic acid. The butanal conversion after 15 min reaction

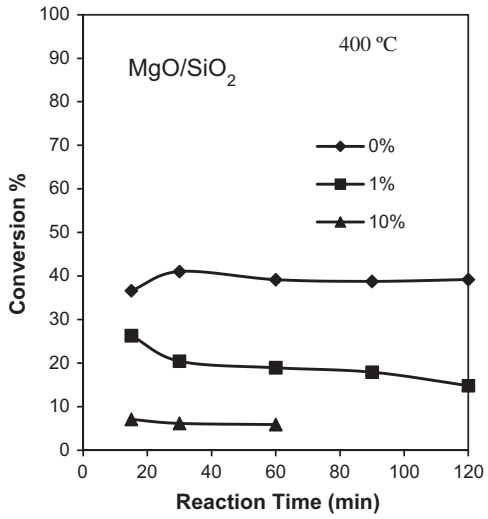


**Fig. 4.** Time-on-stream butanal conversion over the $MgO/SiO_2$ catalyst with co-feed of butanoic acid (vol.%). The reactions were conducted at 400 °C in a 60 mL/min helium flow. Liquid feeding rate was 1.2 mL/h, and catalyst loading was 200 mg.

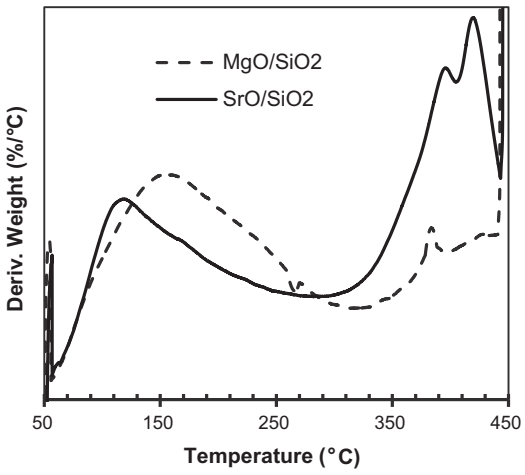


**Fig. 5.** Derivative weight loss over the butanoic acid saturated $MgO/SiO_2$ and $SrO/SiO_2$ as a function of reaction temperature.

decreased from 17.4% without butanoic acid co-feed to 4.9% at 15 min with the 1 vol.% butanoic acid co-feed. After 2 h, the catalyst was almost completely deactivated with the 1 vol.% butanoic acid in butanal feed, whereas the butanal conversion was maintained at 5.1% without co-feed of butanoic acid. At 400 °C, the butanal conversion decreased from about 40% to about 20% with 1 vol.% of butanoic acid in the butanal feed to less than 10% with 10 vol.% butanoic acid in the butanal feed. The catalyst apparent deactivation rate increased from 0.00014 $min^{-1}$ to 0.0042 $min^{-1}$ and 0.0016 $min^{-1}$ with co-feeds of 0 vol.%, 1 vol.% and 10 vol.% of butanoic acid, respectively. A shift in the product distribution was also observed with an increase in the yields of heptanone and C7 alkenes. This provided additional evidence that C7 alkenes are produced by ketonization of butanoic acid followed by hydrogenation/dehydration as we proposed in the reaction network. The yield of double adol addition product EOEA decreased from 4% to 2% with 1 vol.% butanoic acid to 0% with 10 vol.% butanoic acid, indicating the reduction of the base strength over $MgO/SiO_2$ due to the co-feed of the organic acid. The results reveal that butanoic acid deactivates the $MgO/SiO_2$ catalyst at the lower operating temperature of 300 °C. At higher temperatures, a small amount of the butanoic acid is able to be converted by ketonization reactions, thus the catalyst can maintain steady-state operation. However, an increase in the butanoic acid concentration in the butanal feed decreased the catalyst activity at all the operating temperatures.

### 3.6. Butanoic acid TPD-TGA

Butanoic acid desorption was studied by temperature programmed desorption. The $MgO/SiO_2$ and $SrO/SiO_2$ catalysts were saturated with butanoic acid vapor at 50 °C and then heated up to 450 °C in a 100 mL/min flow of He. During the TPD, the total weight loss due to the release of butanoic acid was about 8.5 wt.% and 9.6 wt.% over $MgO/SiO_2$ and $SrO/SiO_2$, respectively. The derivative weight loss over the butanoic acid saturated catalysts is in Fig. 5. Two desorption peaks over $MgO/SiO_2$ were observed with one ranging from 50 °C to ~300 °C and the other starting at ~350 °C. The low-temperature peak can be assigned to the release of weakly bonded butanoic acid. The high-temperature peaks can be assigned to strongly bonded butanoic acid. $SrO/SiO_2$ shows a relatively stronger bond to butanoic acid with more weight loss at higher temperatures. The TPD experiment reveals that butanoic acid can be strongly absorbed onto the surface of $MgO/SiO_2$ and $SrO/SiO_2$. At temperatures close to 300 °C, there is

**Table 5**
Butanal conversion, catalyst apparent deactivation rate and product selectivity over $MgO/SiO_2$ with co-feed of butanoic acid.

| Catalyst | Acid in feed (vol.%) | Reaction time (min) | Butanal conversion (%) | Apparent deactivation rate ($min^{-1}$) | Product yield (%) | | | | | | | | | |
|---|---|---|---|---|---|---|---|---|---|---|---|---|---|---|
| | | | | | EHEA | C7AL | DC8AL | BA | HPO | EHEO | EHAA | BBR | TEB | EOEA |
| MgO/$SiO_2$ | 0 | 15 | 17.4 | 0.0067 | 14.6 | – | – | – | 0.05 | 1.39 | 0.07 | – | – | 1.51 |
| (300 °C) | | 120 | 5.1 | | 4.4 | – | – | 0.05 | 0.04 | 0.35 | 0.07 | – | – | – |
| MgO/$SiO_2$ | 1 | 15 | 4.9 | 0.0089 | 3.9 | – | – | – | – | 0.34 | 0 | – | – | 0.43 |
| (300 °C) | | 120 | 0.5 | | 0.5 | – | – | – | – | – | – | – | – | – |
| MgO/$SiO_2$ | 0 | 15 | 40.6 | 0.00014 | 18.8 | 0.89 | 2.96 | – | 0.97 | 3.37 | 0.93 | – | 0.12 | 4.06 |
| (400 °C) | | 120 | 40.0 | | 23.0 | 0.64 | 1.68 | – | 1.32 | 4.08 | 0.84 | – | 0.40 | 3.56 |
| MgO/$SiO_2$ | 1 | 15 | 26.3 | 0.0042 | 15.6 | 1.00 | 0.79 | – | 1.00 | 2.50 | 0.32 | – | 0.08 | 2.16 |
| (400 °C) | | 120 | 14.8 | | 10.1 | 0.75 | – | – | 0.96 | 1.70 | 1.72 | – | – | 0.47 |
| | 10 | 15 | 7.1 | 0.0016 | 2.7 | 0.90 | – | – | 1.60 | 0.37 | – | – | 0.13 | – |
| | | 60 | 5.9 | | 1.3 | 0.58 | – | – | 2.01 | – | – | – | 0.10 | – |

*Note*: The product of BA is not shown here for the reactions with co-feed of butanoic acid.
EHEA: 2-ethyl-2-hexenal; C7AL: C7 alkanes; C8AL: C8 alkanes; BA: butanoic acid; HPO: heptanone; EHEO: 2-ethyl-2-hexenol; EHAA: 2-ethyl-hexanal; TEB: triethyl benzene; EOEA: 2,4-diethyl-2,4-octadienal.

still a significant amount of absorbed butanoic acid, which competes with butanal and occupies the active sites, thus leading to the deactivation of the catalyst. By increasing the reaction temperature to above 350 °C, the butanoic acid will either decompose or react forming heptanone, a compound that might be weakly bonded to the surface of the catalyst. The result of the TPD experiment is consistent with our kinetic studies, showing that temperatures above 350 °C are required to remove butanoic acid from the catalyst surface.

### 3.7. Butanal-TPD-DRIFTS

In situ DRIFTS infrared spectroscopy was used to study the reaction intermediates and the catalyst deactivation of butanal and butanoic acid over the catalysts. A TPD type experiment was undertaken by first adsorbing the reactant vapor onto the catalysts surface and following the surface reaction using infrared spectroscopy, with increasing temperature under a flow of inert gas (He). Fig. 6 shows the TPD-DRIFTS spectra of butanal adsorption over $MgO/SiO_2$ in the hydroxyl group region (4000–3200 $cm^{-1}$), the C—H stretching region (3200–2400 $cm^{-1}$) and the finger print region (1800–1200 $cm^{-1}$). Due to the strong absorbance from the silica support, the spectra below ~1500 $cm^{-1}$ show poor signal-to-noise ratio. Therefore, the reaction intermediates during the TPD are difficult to identify. Here, we only discuss the vibrations above 1500 $cm^{-1}$. The in situ DRIFTS spectrum of the calcined $MgO/SiO_2$ before butanal sorption shows two hydroxyl bands: a sharp band at 3742 $cm^{-1}$ assigned to the free hydroxyl groups from both the silica support and magnesia and a broad band at 3666 $cm^{-1}$ attributed to the hydroxyl groups from silica-magnesia mixed oxide such as talc and forsterites [49]. After butanal adsorption and evacuation, the free hydroxyl band at 3742 $cm^{-1}$ is significantly decreased in intensity and slightly shifted to lower wavenumber of 3738 $cm^{-1}$, indicating that the free hydroxyl groups were involved in the adsorption process. In addition, a broad hydroxyl band at ~3400 $cm^{-1}$ appeared in the spectrum, which can be assigned to the vibrations of associated O—H groups due to the water formation from the dehydration of the aldol product. The band at 3666 $cm^{-1}$ was not affected by increasing the temperature, which might be explained in that the hydroxyl groups that give rise to the band at 3666 $cm^{-1}$ were not accessible to the butanal molecules. With increasing temperature, the new band at 3400 $cm^{-1}$ disappeared at 200 °C. This suggests that this band does indeed involve strongly adsorbed water. The intensity of the band at 3738 $cm^{-1}$ increased with increasing temperature, indicating the free hydroxyl groups were regenerated after butanal or reaction products desorption.

The bands at 2970 $cm^{-1}$, 2943 $cm^{-1}$ and 2884 $cm^{-1}$ can be assigned to $\nu_{as}(CH_3)$, $\nu_s(CH_3)$ and $2\nu_6A'$ Fermi for absorbed butanal, respectively (with reference to acetaldehyde over silica [56]). These bands decreased with increasing temperature. The weak band at 2740 $cm^{-1}$ can be assigned to the $\nu(CH)_{aldehyde}$ vibration, and this band completely disappeared at 200 °C. The sharp band at 1740 $cm^{-1}$ is due to the vibration of $\nu$(C=O). The band at 1640 $cm^{-1}$ is attributed to unsaturated aldehyde $\nu$(C=C), and the broad band at 1590 $cm^{-1}$ can be attributed to the formation of coke [29,53]. Since C=C bonds and water are observed at 50 °C, it can be concluded that the aldol condensation of butanal on the surface of

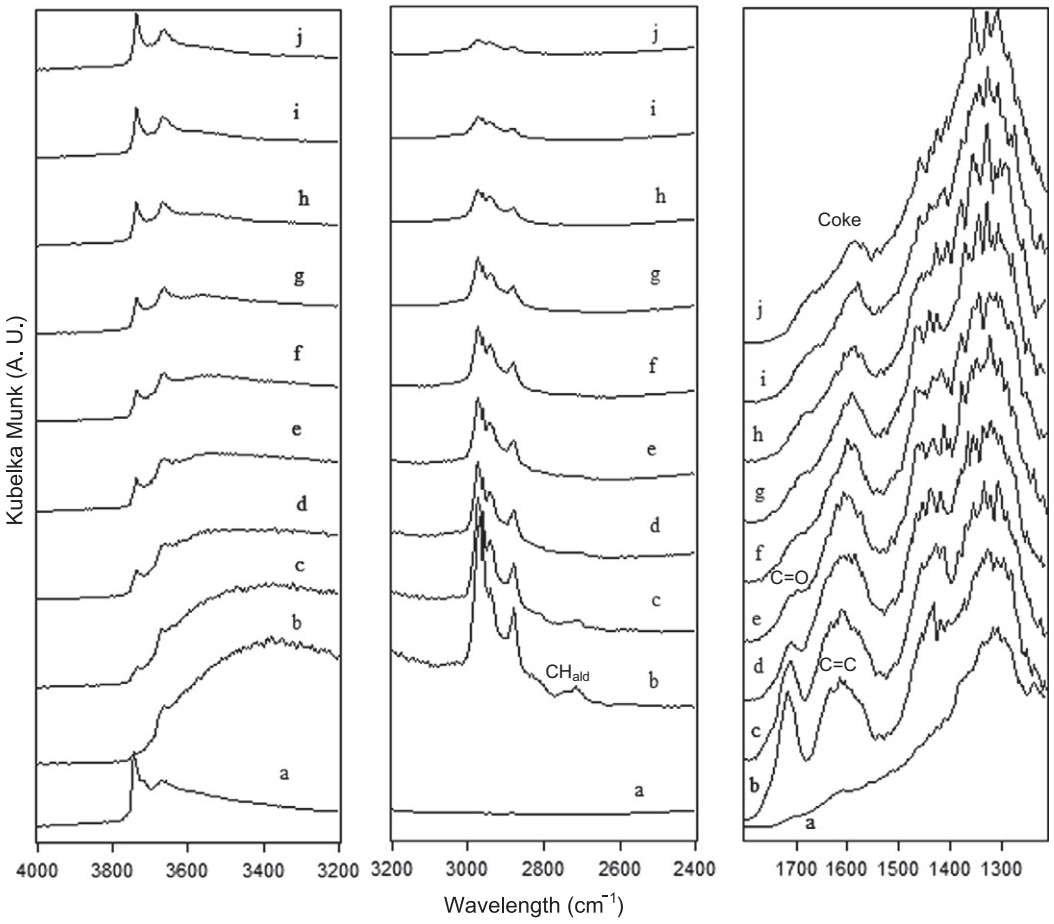


**Fig. 6.** DRIFTS spectra of butanal absorbed on $MgO/SiO_2$ at different temperatures: (a) $MgO/SiO_2$ before butanal absorption; (b) 50 °C; (c) 100 °C; (d) 150 °C; (e) 200 °C; (f) 250 °C; (g) 300 °C; (h) 350 °C; (i) 400 °C; (j) 450 °C.

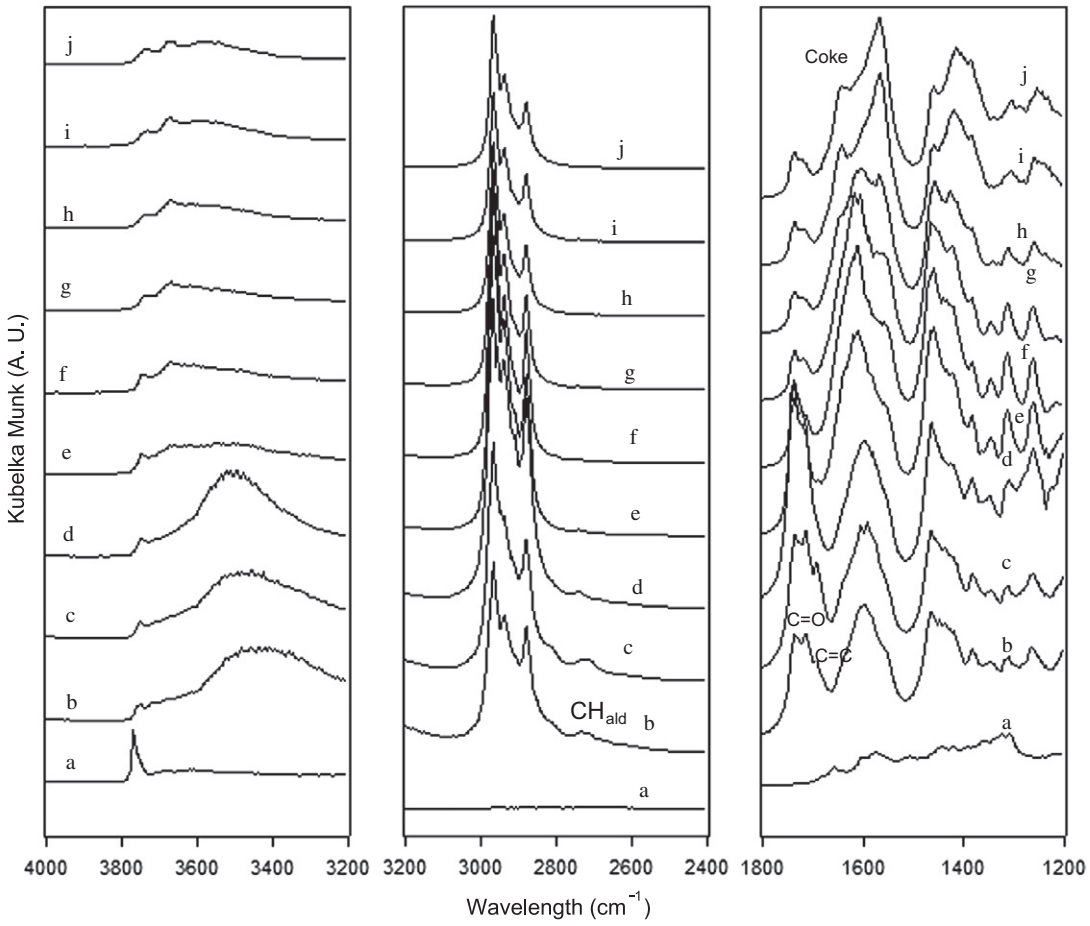


**Fig. 7.** DRIFTS spectra of butanal absorbed on MgO at different temperatures: (a) MgO before butanal absorption; (b) 50 °C; (c) 100 °C; (d) 150 °C; (e) 200 °C; (f) 250 °C; (g) 300 °C; (h) 350 °C; (i) 400 °C; (j) 460 °C.

$MgO/SiO_2$ occurs at a temperature of 50 °C. The adsorbed butanal and the aldol addition product (mainly $\nu(CH)_{ald}$ and $\nu(C{=}O)$) disappeared at 200–250 °C. The residue strongly adsorbed species contributed to the formation of coke at temperatures above 350 °C.

Fig. 7 shows the TPD-DRIFTS spectra of butanal adsorption over MgO in the hydroxyl group stretching region, the C—H stretching region and the region between 1800 and 1200 cm$^{-1}$. The surface hydroxyl groups on MgO have been extensively studied [57–59]. There are four types of hydroxyl groups on the MgO surface related to $Mg^{2+}_{LC} - O^{2-}_{LC}$ pairs, including isolated hydroxyls on $Mg^{2+}$ (A), isolated multicoordinated hydrogen bonded with $O^{2-}$ (type B), monocoordinated hydrogen-bond acceptor (type C) and multicoordinated hydrogen-bond donor (type D). Over the fresh MgO catalyst, the sharp band at 3770 cm$^{-1}$ can be assigned to the free type A hydroxyl groups, while the broad band at 3610 cm$^{-1}$ can be assigned to the type D hydroxyl groups over MgO. After butanal adsorption and evacuation, both hydroxyl groups over MgO were perturbed. The band at 3770 cm$^{-1}$ was significantly weaker in intensity and shifted to 3750 cm$^{-1}$, and a new broad band at 3400 cm$^{-1}$ appeared due to the $\nu_{OH}$ vibrations of associated OH-groups [60]. With increasing temperature, the band at 3400 cm$^{-1}$ shifted to high wavelength of 3500 cm$^{-1}$ at 150 °C and disappeared at 200 °C. A new band at 3670 cm$^{-1}$ appeared at temperatures above 200 °C, and the intensity of this band increased with increasing temperature. The surface hydroxyl groups over MgO changed completely with butanal adsorption and sequential desorption at elevated temperatures, indicating the strong interaction and surface reactions occurred with the adsorbed species. The results are quite different from the observation of $MgO/SiO_2$ butanal-TPD, where the surface hydroxyl groups are involved in the adsorption process, but most of the sites can be recovered from poison desorption at higher temperatures.

Similar with the butanal-TPD over $MgO/SiO_2$, the aldehyde C—H stretching band, $\nu(CH)_{ald}$, at 2735 cm$^{-1}$ disappeared at 200 °C. The bands at 1736 cm$^{-1}$ and 1713 cm$^{-1}$ can be assigned to the stretching vibration of the carbonyl group $\nu(C{=}O)$ due to the absorbed butanal and/or the reaction intermediates [27,61], and the band at 1672 cm$^{-1}$ was assigned to $\nu(C{=}C)$ from 2-ethyl-2-hexenal [27,29,56,61]. The intensity of C=O and C=C bands increased to a maximum at 150 °C and decreased with further increasing temperature. The absorbed water band at 3400 cm$^{-1}$ shifted to 3500 cm$^{-1}$ at 150 °C along with the increase intensity of C=O and C=C stretching bands, indicative of side reactions other than the aldol condensation reaction occurred. Further increasing the temperature to above 200 °C, the C=O band significantly decreased in intensity. Compared to $MgO/SiO_2$, significantly more residues were observed on the MgO surface at 460 °C, including carbonaceous species and coke or its precursors, which were strongly bonded with the catalyst surface.

The butanal-TPD experiment over both MgO and $MgO/SiO_2$ gave us insight into the catalytic surface chemistry. The MgO catalyst surface was covered with significant amounts of carbonaceous species that occupied the active sites at elevated temperatures due to strong interaction of the butanal and its products with the MgO surface. These products therefore deactivated the catalyst surface. However, there was only a small amount of coke formed on the

$MgO/SiO_2$ surface. Thus, the silica supported MgO catalyst had a much longer lifetime for vapor phase butanal condensation at reaction temperatures above 350 °C. At the lower reaction temperature of 300 °C, the $MgO/SiO_2$ catalyst deactivated due to the strong adsorption of butanoic acid produced from the side reactions as discussed in Section 3.6.

### 3.8. Design of acid–base bifunctional solid catalysts for aldehyde and ketone condensation

In this paper, we have demonstrated that silica supported MgO, SrO and mixed MgO—SrO were active for vapor phase butanal condensation and stable at temperatures above 350 °C. In contrast, MgO showed low activity and poor stability. The butanal-TPD-DRIFTS revealed that MgO can catalyze butanal aldol condensation. However, the interaction of adsorbed species with the pure MgO surface is very strong, thus the produced products cannot be desorbed from the catalyst surface. Di Cosimo and Apesteguía [20] studied the catalyst deactivation over MgO and the alkaline earth promoted MgO catalysts in vapor phase acetone condensation. It was found that MgO-based catalysts deactivated due to blockage of basic sites by heavily oligomeric compounds formed from aldol condensation, consistent with our experimental results. The stronger the basicity of the promoted metal oxide, the more quickly the catalyst deactivated. Ji and coworker [31] showed that the super acidic sites on sulfate modified $ZrO_2$ led to the formation of coke with little selectivity toward aldol condensation. Therefore, the ideal catalysts for vapor phase aldehyde and ketone condensation should be neither a strong acid nor a strong base, but have a combination of acid and basic sites.

Numerous studies showed that the aldol condensation reaction was facilitated by acid–base bifunctional catalysts [39–41,62,54]. The acid and base property of silica and alumina supported cesium oxide has been studied by Tai and Davis [41] for vapor phase aldol condensation of propionic acid with formaldehyde, and they found that the reaction was promoted by a combination of Brønsted acid sites with base sites. Climent and coworkers [39] revealed that the weak acid sites activated the vapor phase aldehyde by interaction with the carbonyl group, facilitating the attack of the enolate intermediate generated on the relatively weak basic sites. Furthermore, Spivey and coworker [54] stated that the catalysts that exhibited high condensation yields in vapor phase condensation had characteristic low-temperature $CO_2$ and $NH_3$-TPD desorption peaks in the range of 50–300 °C and the absence of a high-temperature desorption peak at 300–550 °C. In addition, the activity was related to the ratio of the weak acid/base sites. Thus, acid–base bifunctional catalysts with moderate acid/base strength are desired for vapor phase aldol condensation. Our characterization results indicated that the addition of the $SiO_2$ to MgO and SrO caused a decrease in the concentration of strong basic sites and the formation of acidic sites. This facilitated the aldol condensation reaction over silica supported alkaline metal oxides.

Considering the self-poisoning of the catalysts by acid by-products for aldehyde condensation, the ideal catalyst should also possess a surface that weakly bonds with carboxylic acid or the surface is catalytically active for the ketonization reaction. Rare earth metal oxides, for example, $CeO_2$ and $La_2O_3$, are well known for their acid and base nature [63]. And the ceria-based catalysts have been studied [11,64,65] for carboxylic acid ketonizations with high activity. Recently, Kunkes et al. [8] conducted gas phase 2-hexanone self-condensation/hydrogenation reactions over a $Pd/CeZrO_x$ catalyst at 300–400 °C. The catalyst showed high activity for C—C bond formation reactions. Therefore, we might foresee that the silica supported ceria or ceria-based catalysts are excellent catalysts for vapor phase aldol condensation. More work is required to tune the acid/base properties of the catalyst surface by changing the metal oxide loading, the support and the metal oxide composition for vapor phase condensation reaction, particularly, to reduce the acid strength for the elimination of coke formation and to determine the relationship between the acid/base sites and the catalytic activity.

## 4. Conclusions

Vapor phase butanal self-condensation reaction was studied over silica supported and unsupported MgO and SrO, in a fixed-bed flow reactor. The strong solid base MgO catalyst showed low activity and stability. The silica supported MgO, SrO and MgO—SrO and MgO/HY had significantly higher initial catalytic activity. However, the supported catalysts deactivated quickly at 300 °C due to poisoning by butanoic acid. Increasing the reaction temperature to above 350 °C, the $MgO/SiO_2$ and $SrO/SiO_2$ catalysts became relatively stable and the butanal conversion increased from 17% to 24%. Butanoic acid was no longer detected in the effluent at these higher temperatures. More heptanone and C7 alkenes were generated at higher temperatures through butanoic acid ketonization reaction followed by hydrogenation/dehydration reactions. Further increasing the reaction temperature to 400 °C increased the butanal conversion to 40%. $SrO/SiO_2$ showed relatively higher selectivity to the aldol addition product EHEA. Co-feeding the butanoic acid inhibited the catalytic performance of $MgO/SiO_2$ due to the strong adsorption of the butanoic acid. Butanal conversion was reduced from 40% to 26% to 7% with co-feed of 1 vol.% and 10 vol.% butanoic acid, respectively, over $MgO/SiO_2$ at 400 °C. The reaction network for vapor phase butanal condensation was also proposed. The primary reaction pathway is butanal aldol condensation followed by dehydration for EHEA. This reaction competes with Tishchenko-type esterification reactions. The cross-esterification between EHEA and butanal is preferred to the butanal self-esterification reaction. Other side reactions include double aldol addition, ester hydrolysis, ketonization, isomerization, cyclization, hydrogenation and dehydration.

X-ray diffraction of the catalysts showed that silica supported MgO, SrO and MgO—SrO catalysts are amorphous, indicating that the alkaline earth metal oxides were well dispersed into silica support or form amorphous silicate compounds. The $CO_2$- and $NH_3$-TPD showed that the base strength was much weakened and the number of base sites was dramatically reduced over the supported alkaline earth metal oxides. In addition, new acid sites were generated over silica supported catalysts as suggested by the strong $NH_3$ sorption. Butanal-TPD-DRIFTS experiments over MgO and $MgO/SiO_2$ showed significant differences between these two catalysts. The surface of $MgO/SiO_2$ showed a relatively weak interaction with adsorbed species, and most of the surface hydroxyl groups could be recovered upon increasing the reaction temperature. A small amount of coke was formed on the catalyst surface at elevated temperature, which contributes to the slight deactivation of the $MgO/SiO_2$ catalyst at high temperature. In contrast, the MgO surface showed a strong interaction with butanal and the reaction intermediates. The catalyst was covered by significant amount of carbonaceous species and coke, contributing to the low activity and short lifetime. The butanoic acid TPD-TGA experiment revealed that both $SrO/SiO_2$ and $MgO/SiO_2$ had very strong bonding with butanoic acid. The butanoic acid was converted by Ketonization reaction when the temperature was increased above 350 °C. The acid/base properties of alkaline earth metal oxides can be tuned by the addition of the silica support that facilitated the vapor phase aldol condensation reaction and reduced the coke formation. The ideal catalyst comprises a combination of moderate strength acidic and basic sites.

## Acknowledgements

The author would like to thank for the financial support from the United States Department of Energy (DOE) (DE-FG02-07ER15918 and DE-FG02-96ER14681), and an NSF-MRI Grant (0722802).

## Appendix A. Supplementary material

Supplementary data associated with this article can be found, in the online version, at doi:10.1016/j.jcat.2011.11.009.

## References

[1] G.W. Huber, R.D. Cortright, J.A. Dumesic, Angew. Chem., Int. Ed. 43 (2004) 1549.
[2] G.W. Huber, J.N. Chheda, C.J. Barrett, J.A. Dumesic, Science 308 (2005) 1446.
[3] R.M. West, E.L. Kunkes, D.A. Simonetti, J.A. Dumesic, Catal. Today 147 (2009) 115.
[4] R. Xing, A.V. Subrahmanyam, H. Olcay, W. Qi, G.P. van Walsum, H. Pendse, G.W. Huber, Green Chem. 12 (2010) 1933.
[5] D.A. Simonetti, J.A. Dumesic, ChemSusChem 1 (2008) 725.
[6] E.L. Kunkes, D.A. Simonetti, R.M. West, J.C. Serrano-Ruiz, C.A. Gartner, J.A. Dumesic, Science 322 (2008) 417.
[7] E.I. Gurbuz, E.L. Kunkes, J.A. Dumesic, Green Chem. 12 (2010) 223.
[8] E.L. Kunkes, E.I. Gürbüz, J.A. Dumesic, J. Catal. 266 (2009) 236.
[9] W. Shen, G.A. Tompsett, K.D. Hammond, R. Xing, F. Dogan, C.P. Grey, W.C. Conner Jr., S.M. Auerbach, G.W. Huber, Appl. Catal. A 392 (2011) 57.
[10] C.A. Gaertner, J.C. Serrano-Ruiz, D.J. Braden, J.A. Dumesic, J. Catal. 266 (2009) 71.
[11] C.A. Gärtner, J.C. Serrano-Ruiz, D.J. Braden, J.A. Dumesic, ChemSusChem 2 (2009) 1121.
[12] R.N. Hayes, R.P. Grese, M.L. Gross, J. Am. Chem. Sci. 111 (1989) 8336.
[13] L.M. Baigrie, R.A. Cox, H. Slebocka-Tilk, M. Tencer, T.T. Tidwell, J. Am. Chem. Sci. 107 (1985) 3640.
[14] G. Zhang, H. Hattori, K. Tanabe, Appl. Catal. 36 (1988) 189.
[15] J.I. Di Cosimo, V.K. Díez, C.R. Apesteguía, Appl. Catal. A 137 (1996) 149.
[16] M. Zamora, T. López, M. Asomoza, R. Meléndrez, R. Gómez, Catal. Today 116 (2006) 234.
[17] M. Zamora, T. López, R. Gómez, M. Asomoza, R. Meléndrez, Appl. Surf. Sci. 252 (2005) 828.
[18] M. Paulis, M. Martín, D.B. Soria, A. Díaz, J.A. Odriozola, M. Montes, Appl. Catal. A 180 (1999) 411.
[19] A.S. Canning, S.D. Jackson, E. McLeod, E.M. Vass, Appl. Catal. A 289 (2005) 59.
[20] J.I. Di Cosimo, C.R. Apesteguía, J. Mol. Catal. A: Chem. 130 (1998) 177.
[21] W.T. Reichle, J. Catal. 94 (1985) 547.
[22] S. Lippert, W. Baumann, K. Thomke, J. Mol. Catal. 69 (1991) 199.
[23] H. Tsuji, F. Yagi, H. Hattori, H. Kita, J. Catal. 148 (1994) 759.
[24] F. King, G.J. Kelly, Catal. Today 73 (2002) 75.
[25] S.K. Sharma, P.A. Parikh, R.V. Jasra, J. Mol. Catal. A: Chem. 278 (2007) 135.
[26] E. Dumitriu, V. Hulea, I. Fechete, A. Auroux, J.-F. Lacaze, C. Guimon, Micropor. Mesopor. Mater. 43 (2001) 341.
[27] Y.-C. Chang, A.-N. Ko, Appl. Catal. A 190 (2000) 149.
[28] E. Dumitriu, V. Hulea, N. Bilba, G. Carja, A. Azzouz, J. Mol. Catal. 79 (1993) 175.
[29] E.J. Rode, P.E. Gee, L.N. Marquez, T. Uemura, M. Bazargani, Catal. Lett. 9 (1991) 103.
[30] B.J. Arena, J.S. Homgren, US Patent, 5 144 089, 1991 (to UOP).
[31] W. Ji, Y. Chen, H.H. Kung, Appl. Catal. A 161 (1997) 93.
[32] P. Moggi, G. Albanesi, Appl. Catal. 68 (1991) 285.
[33] H. Idriss, C. Diagne, J.P. Hindermann, A. Kiennemann, M.A. Barteau, J. Catal. 155 (1995) 219.
[34] H. Idriss, K.S. Kim, M.A. Barteau, J. Catal. 139 (1993) 119.
[35] S. Luo, J.L. Falconer, J. Catal. 185 (1999) 393.
[36] H. Madhavaram, H. Idriss, J. Catal. 224 (2004) 358.
[37] G. Zhang, H. Hattori, K. Tenabe, Bull. Chem. Soc. Jpn. 62 (1989) 2070.
[38] F. King, G.J. Kelly, E.H. Stitt, in: M. Anpo, M. Onaka, H. Yamashita (Eds.), Studies in Surface Science and Catalysis, vol. 145, Elsevier, 2003, pp. 443–446.
[39] M.J. Climent, A. Corma, V. Fornés, R. Guil-Lopez, S. Iborra, Adv. Synth. Catal. 344 (2002) 1090.
[40] M.J. Climent, A. Corma, S. Iborra, A. Velty, J. Mol. Catal. A 182–183 (2002) 327.
[41] J. Tai, R.J. Davis, Catal. Today 123 (2007) 42.
[42] A. Azzouz, D. Messad, D. Nistor, C. Catrinescu, A. Zvolinschi, S. Asaftei, Appl. Catal. A 241 (2003) 1.
[43] D.G. Rethwisch, J.A. Dumesic, Langmuir 2 (1986) 73.
[44] M.B. Jensen, L.G.M. Pettersson, O. Swang, U. Olsbye, J. Phys. Chem. B 109 (2005) 16774.
[45] V.K. Díez, C.R. Apesteguía, J.I. Di Cosimo, J. Catal. 240 (2006) 235.
[46] G. Busca, Phys. Chem. Chem. Phys. 1 (1999) 723.
[47] T. López, R. Gomez, M.E. Llanos, E. López-Salinas, Mater. Lett. 38 (1999) 283.
[48] J.A. Lercher, H. Noller, J. Catal. 77 (1982) 152.
[49] G. Ritter, H. Noller, J.A. Lercher, J. Chem. Soc., Faraday Trans. 78 (1982) 2239.
[50] S.V. bordawekar, E.J. Doskocil, R.J. Davis, Langmir 14 (1998) 1734–1738.
[51] J. Shen, R.D. Cortright, Y. chem, J.A. Dumesic, J. Phys. Chem. 98 (1994) 8067–8073.
[52] R.K. Zeidan, M.E. Davis, J. Catal. 247 (2007) 379–382.
[53] R.J. Gorte, Catal. Today 28 (1996) 405–414.
[54] J.J. Spivey, M.R. Gogate, J.R. Zoeller, R.D. Colberg, Ind. Eng. Chem. Res. 36 (1997) 4600.
[55] H. Idriss, K.G. Pierce, M.A. Barteau, J. Am. Chem. Soc. 116 (1994) 3063.
[56] V.V. Ordomsky, V.L. Sushkevich, I.I. Ivanova, J. Mol. Catal. A: Chem. 333 (2010) 85.
[57] E. Knözinger, K.-H. Jacob, S. Singh, P. Hofmann, Surf. Sci. 290 (1993) 388.
[58] C. Chizallet, G. Costentin, M. Che, F. Delbecq, P. Sautet, J. Am. Chem. Soc. 129 (2007) 6442.
[59] R. Echterhoff, E. Knözinger, Surf. Sci. 230 (1990) 237.
[60] G.A.H. Mekhemer, S.A. Halawy, M.A. Mohamed, M.I. Zaki, J. Catal. 230 (2005) 109.
[61] U. Rymsa, M. Hunger, J. Weitkamp, Stud. Surf. Sci. Catal. 135 (2001) P23.
[62] R.K. Zeidan, M.E. Davis, J. Catal. 247 (2007) 379.
[63] A. Auroux, A. Gervasini, J. Phys. Chem. 94 (1990) 6371.
[64] K.M. Dooley, A.K. Bhat, C.P. Plaisance, A.D. Roy, Appl. Catal. A 320 (2007) 122.
[65] O. Nagashima, S. Sato, R. Takahashi, T. Sodesawa, J. Mol. Catal. A: Chem. 227 (2005) 231.